Solar Energy 162 (2018) 265–277

Contents lists available at ScienceDirect

Solar Energy

journal homepage: www.elsevier.com/locate/solener

Solar irradiance forecasting in the tropics using numerical weather prediction and statistical learning

Hadrien Verbois[a,b,c,*], Robert Huva[b], Andrivo Rusydi[a,b,c], Wilfred Walsh[b]

[a] NUS Graduate School for Engineering and Integrative Science, National University of Singapore, Singapore
[b] Solar Energy Research Institute, National University of Singapore, Singapore
[c] Department of Physics, National University of Singapore, Singapore

ABSTRACT

Increasing penetration of distributed renewable power means that reliable generation forecasts are required for grid operation. The present work aims at combining state of the art implementations of the Weather Research and Forecasting (WRF) model with multivariate statistical learning techniques to provide the most accurate forecasts of day-ahead hourly irradiance in Singapore.

Three implementations of WRF-including WRF-solar-were used to produce three years of hourly day-ahead irradiance forecasts. Their performances were compared with that of the Global Forecasting System (GFS), which was interpolated to provide hourly forecasts. A multivariate post-processing procedure combining Principal Component Analysis (PCA) and stepwise variable selection was developed and applied to the four models. A smart persistence model and a climatological forecast were also implemented and served as benchmarks.

The skill of the various models were evaluated using several metrics and statistical tests. We found that WRF-solar combined with our proposed statistical learning method outperformed smart persistence, a climatological forecast and GFS for day-ahead forecasts of irradiance. In particular, our model was shown to have a Root Mean Square Error (RMSE) 23% lower than smart persistence.

1. Introduction

Recent years have seen a dramatic increase in the part of renewables in our energy mix. However, due to the inherent variability of solar irradiance and wind, increasing the penetration of distributed renewable power also means that reliable generation forecasts are required for grid operation. Intra-hour, intra-day, and day-ahead forecasts are needed for grid balancing, power generation and dispatch planning, and for unit commitment and day-ahead energy trading, respectively. Martinez-Anido et al. (2016) showed that for the US grid, accurate prediction of the solar irradiance could significantly help operators to reduce their costs while Kaur et al. (2016) pointed out the benefits of day-ahead forecasting for energy markets. In India, the Central Electricity Regulatory Commission impose a financial penalty to solar energy producer when they deviate from their scheduled generation.

The main step in forecasting solar power–or at least the most uncertain step–is to estimate solar irradiance at the Earth's surface. For intra-hour and intra-day forecasts, time series and machine learning techniques have proven to be most efficient (Inman et al., 2013). Cloud retrievals and satellite imagery can also be coupled with radiation transfer models (RTM) to produce reliable forecasts up to 5 or 6 h ahead (Diagne et al., 2013). But for day-ahead predictions, the processes driving the evolution of the atmosphere are too uncorrelated with current conditions to be resolved by purely statistical methods. Lorenz et al. (2009a) showed that for this horizon, Numerical Weather Prediction models (NWP) yield the best results.

The first operational NWP was set-up in 1954 (Lynch, 2008). Since then, there have been considerable improvements, partly thanks to the manifold increase in available computer power. Accurately forecasting surface irradiance remains nevertheless an ongoing research topic. During the mid-2000s, Zamora et al. (2005), Guarnieri et al. (2006) and Lorenz et al. (2009b) first implemented systematic forecasts of solar irradiance and power using NWP. Since then, several large-scale studies have been conducted to investigate the potential of day-ahead surface irradiance forecasts using NWP in Europe and North America (Mathiesen and Kleissl, 2011; Lara-Fanego et al., 2012b; Perez et al., 2013; Pelland et al., 2013). Tropical regions have been less studied and are more challenging. Tropical weather is harder to forecast and predicting cloud cover is particularly difficult. This is partly due to the importance of resolving convective clouds in these regions, which can

* Corresponding author at: Solar Energy Research Institute of Singapore (SERIS), National University of Singapore (NUS), 7 Engineering Drive 1, Singapore 117574, Singapore.
E-mail address: hadrien@u.nus.edu (H. Verbois).

https://doi.org/10.1016/j.solener.2018.01.007
Received 6 September 2017; Received in revised form 18 December 2017; Accepted 4 January 2018

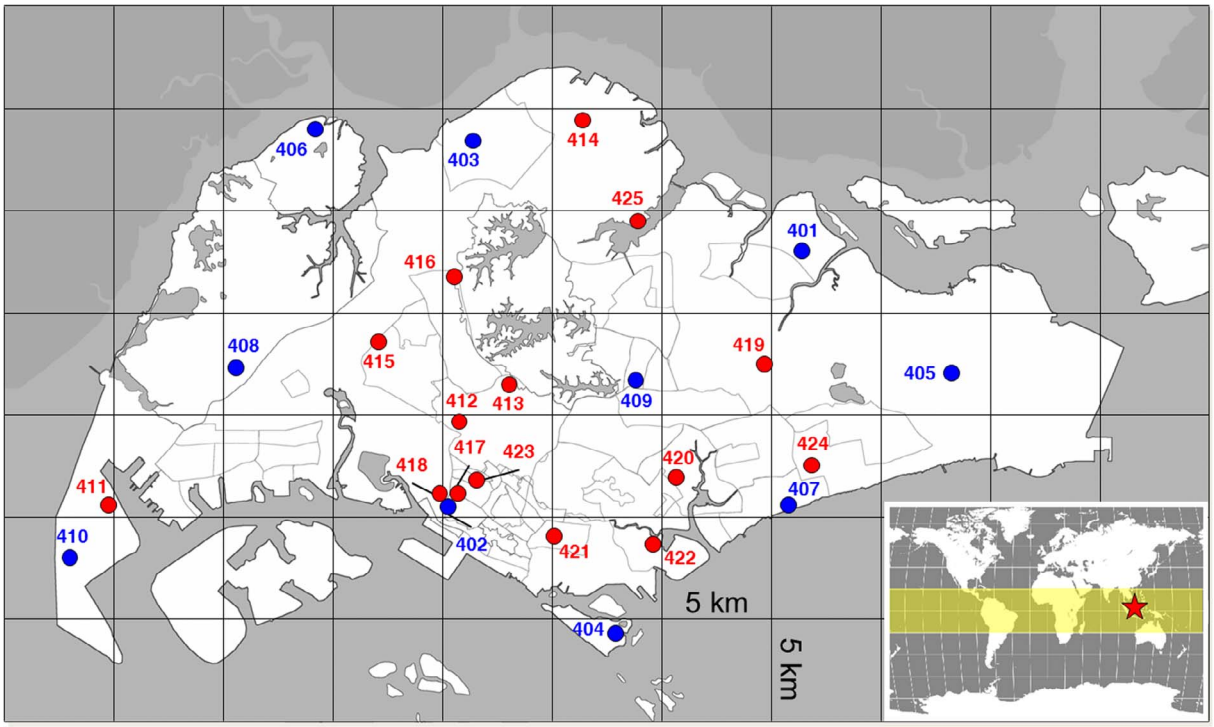

Fig. 1. SERIS network of meteorological stations operational since May 2013.

only be resolved at high spatial resolution. Applying a 3 km grid size, Diagne et al. (2014) used NWP to predict day-ahead solar irradiance in Reunion Island. Similarly, Lima et al. (2016) applied a 5 km grid side NWP model to Brazil. While promising, their forecasts remained biased. Aryaputera et al. (2015) implemented a 1 km grid size NWP for Singapore, but they restricted their study to 60 days which is insufficient to properly represent Singapore weather. In addition, although they showed that WRF performed better at increasingly higher resolutions, their forecasts still exhibited large errors. Somehow unexpectedly, a higher resolution sometimes even lead to larger errors in forecasting irradiance (Lara-Fanego et al., 2012a). For this reason and because of the high computational cost of running a high-resolution NWP, several studies have explored other ways to improve the forecasting of irradiance by NWP. In particular, efforts have been made to improve the parametrisation of sub-grid clouds (Thompson and Eidhammer, 2014; Jimenez et al., 2016), but the results are not yet conclusive and more work needs to be done in that direction. By incorporating the effects of aerosols on the Radiative Transfer Models and on microphysics, Jiménez et al. (2016) were able to significantly improve the irradiance forecasts for clear sky days in the US. The efficacy of this recent parametrisation in a tropical climate still remains to be investigated.

Despite all these improvements, local terrain complexity, uncertain cloud formation physics, and imperfect observational data combine to introduce random and systematic errors in even high-resolution state of the art numerical forecasts (Ruiz-Arias et al., 2016; Pierro et al., 2015). This is why NWP forecasts are often coupled with statistical learning algorithms. The algorithms are designed to learn from past forecasts errors in an attempt to predict the bias of the future NWP predictions. Model Output Statistics (MOS) is a post-processing technique introduced in 1972 by Glahn and Lowry (1972) and can be described in this context as: one or several output variable(s) of a NWP used as dependent variables in a linear regression model with the desired variable as output (solar irradiance in our case). Neural Networks (Lima et al., 2016; Lauret et al., 2014; Cornaro et al., 2015), Kalman Filters (KF) (Diagne et al., 2014) and Bayesian Model Averaging (BMA) (Aryaputera et al., 2016) have also been used to improve NWP irradiance predictions. Although Glahn and Lowry (1972) already suggested in 1972 the potential of MOS for multiple inputs, few truly multivariate algorithms have been developed. Lorenz et al. (2009b) have combined WRF with a multiple linear regression model (MOS) to predict solar irradiance over Germany, but the regressors were selected based on expert knowledge. Only Verzijlbergh et al. (2015) have used a systematic approach to regressor selection for solar irradiance forecasting. They implemented a stepwise selection process to select a small set of regressors from the Global Forecast System (GFS) output.

Our aim in this work is to produce the best possible day-ahead forecast of solar irradiance for Singapore. For that purpose, we have to tackle two problems. Firstly, we want to implement the best possible NWP for the tropical Singaporean weather; we thus compare three different implementations of the Weather Research and Forecasting (WRF) model-including WRF-solar, recently presented by Jiménez et al. (2016). Secondly, we want to combine this physical forecast with a novel statistical learning method: we combine a stepwise variable selection regression with a principal component analysis (PCA) to best benefit from the multivariate nature of WRF output.

This paper is organised as follow. Data and methods are described in Section 2; in particular, we present the WRF implementations used in this work and detail our post-processing method. The results are presented in Section 3; we discuss the performance of our models and compare them to (1) smart persistence, (2) the climatological model and (3) the Global Forecasting System (GFS). A summary of the results and conclusions are given in Section 4.

2. Material and methods

2.1. Study area and observations

Singapore is a city-state located within 2° of the equator, at a longitude of 140° and is largely composed of a single island that covers ca. 700 km^2. It has a typical equatorial climate, with high and relatively invariant temperature and high humidity. The main seasonal phenomena are the northeast and the southwest monsoon winds that blow from December to early March and from June to September respectively. There is no particular wet or dry season and rainfall is abundant

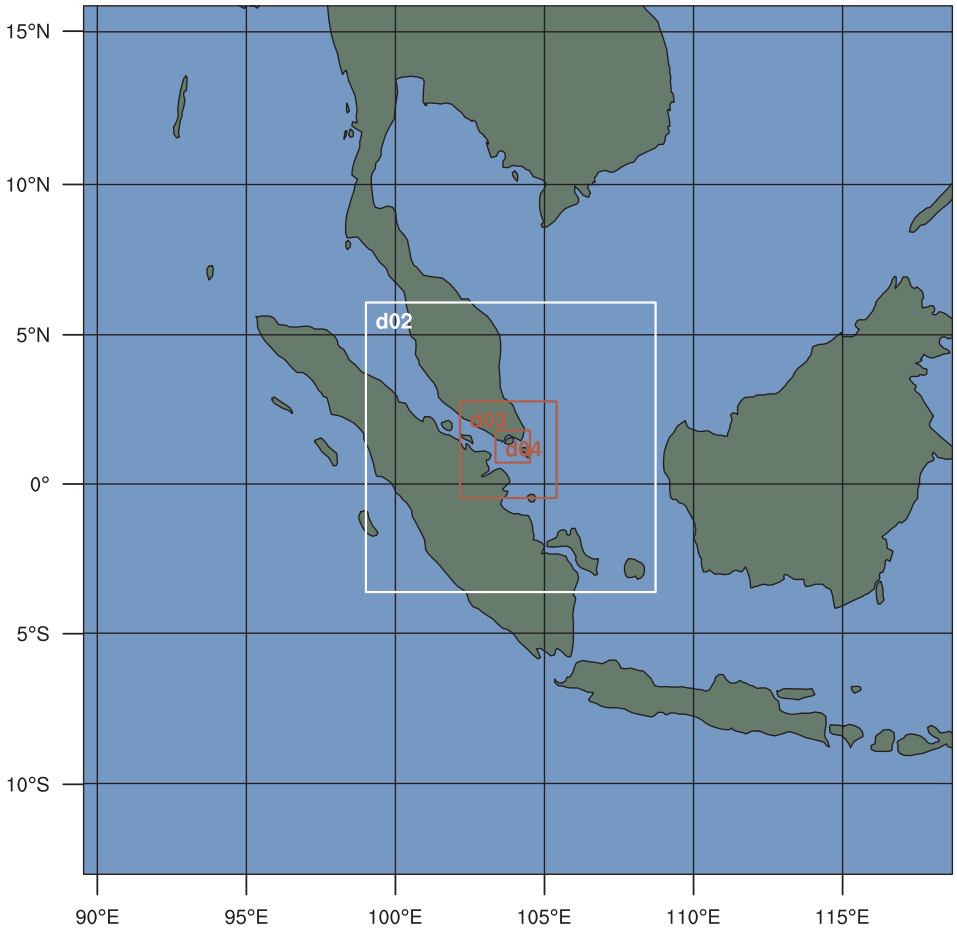

Fig. 2. Domains decomposition of WRF. Domain 1, 2, 3 and 4 have a horizontal spatial resolution of 1, 3, 9 and 27 km respectively; domain 1, 2 and 3 have a grid size of 121 × 121 cells and domain 4 of 130 × 121 cells.

all year long with a peak in April–May, and October–December. The cloud cover often follows a diurnal cycle, with cumulus clouds starting to develop in the mid-morning and growing through the afternoon before diminishing by dusk. Larger scale phenomena, like northeast monsoon surge and Sumatra squall line, also influence the cloud cover. Weather forecasting in equatorial and tropical climate is known to be particularly challenging, mostly due to the instability of the atmosphere in such latitudes.

The Solar Energy Research Institute of Singapore (SERIS) operates a network of 25 meteorological stations across Singapore, illustrated in Fig. 1. Each station measures the Global Horizontal Irradiance (GHI) using a IMT-Solar Si-02-PT-100 silicon sensor at a sampling rate of 1 Hz. Second data are stored locally and transferred through the 3G network to SERIS server where they are stored as 1 min average in a SQL database. A batch retrieval is done every evening to fill any gaps in the database that may be due to network failure. The silicon sensors are calibrated every two years at A*Star National Metrology Center in Singapore and have an accuracy of 5%.

In this study, the evaluation is carried out for 1 h time resolution. The hourly GHI for e.g. 9 am is obtained by averaging minute values from 8:31 am to 9:30 am; hours with missing minute-data are ignored. Furthermore, we are interested in hourly GHI averaged over Singapore, that we extrapolate from the 25 individual stations using the mean of all of them. Finally, only zenith angles below 70° are considered; it corresponds to a window between 9am and 5 pm (with little seasonal variations in Singapore).

2.2. Clear sky index and irradiance

The clear sky index k_t is a good proxy for the sky condition. In this study, k_t is used to deliver a weather-dependent analysis of the performance of the various models, as well as to help the post-processing algorithms to resolve the daily and yearly periodic movements of the sun (see Section 2.4.1). It is defined in the following equation:

$$k_t = \frac{I_t}{I_{t,clear\ sky}} \tag{1}$$

where I_t is the global horizontal irradiance and $I_{t,clear\ sky}$ is the corresponding estimate for the clear sky irradiance. k_t close to 0 indicates a fully overcast sky and k_t equal to–or even slightly higher than–1 indicates a clear sky.

$I_{t,clear\ sky}$ is estimated using an empirical clear sky model, as proposed for Singapore by Yang et al. (2014):

$$I_{t,clear\ sky} = aE_0 I_{sc} (cos(\theta_t))^b e^{c(90-\theta_t)} \tag{2}$$

where I_{sc}, θ_t and E_0 are the solar constant, the solar zenith angle, and the eccentricity correction factor of earth, respectively, and a, b, and c are parameters that are fitted to one year of GHI measurements. For more details about this model, we refer the reader to Yang et al. (2014).

2.3. Numerical Weather Prediction (NWP)

2.3.1. The Weather Research and Forecasting model (WRF)

The Weather Research and Forecasting model (WRF) (Skamarock et al., 2008) is a mesoscale Numerical Weather Prediction system, principally developed and maintained by the National Center for Atmospheric Research (NCAR), the National Oceanic and Atmospheric Administration (NOAA) and the National Centers for Environmental Prediction (NCEP). It is open source software and thus benefits from contributions of a large user community. WRF solves the dynamic and thermodynamic equations of the atmosphere using a dynamical solver. In this work, we use version 3.8.1 of the NCAR Advanced Research WRF

(ARW)–where the ARW solver is the most widely used and thus contains most of the recent developments in the WRF community. In addition, WRF runs several physical schemes that simulate phenomena that cannot be resolved by the dynamical solver. These unresolved phenomena can be of three types: the processes that operate on scales too small to be resolved by WRF grid (e.g. shallow convective clouds); the processes involving an exchange of energy, momentum or water between the atmosphere and another source (e.g. radiation from the sun); the processes involved in cloud and precipitation physics. One great strength of WRF is that it offers a large choice of implementations for each physical scheme, allowing the users to tune the model to their needs.

In this work, we evaluate the performance of three different WRF configurations. For all three set-ups, we follow Aryaputera et al. (2015) and use four nests with a horizontal spatial resolution of 27, 9, 3 and 1 km with 1-way-feedback and 35 vertical levels. The domain decomposition is illustrated in Fig. 2; domain 1, 2, and 3 are composed of 121 × 121 cells and domain 4 of 130 × 121 cells. Following Diagne et al. (2014) and Lara-Fanego et al. (2012b), we use the updated Kain-Fritsch cumulus scheme (Kain and Kain, 2004) in the two largest domains only, as convective clouds are expected to be explicitly resolved in the two smallest. All configurations also use the 2nd Mellor-Yamada-Nakanishi-Niino (MYNN2) planetary boundary layer scheme (Nakanishi and Niino, 2006), the unified Noah land-surface model (Ek et al., 2003) and the RRTMG longwave scheme (Iacono et al., 2008).

Our two first configurations, WRF-dudhia and WRF-rrtmg, use the Thomson microphysics scheme and the Dudhia (Dudhia, 1989) and RRTMG (Iacono et al., 2008) shortwave scheme, respectively. Our third configuration, WRF-solar, adopts some of the improvements presented by Jiménez et al. (2016); namely the aerosol aware Thomson microphysics and the aerosol aware RRTMG shortwave scheme. The aerosols are classified into two species: hygroscopic and nonhygroscopic aerosols and their concentrations are initialised from a three-dimensional monthly climatological map provided by the Goddard Chemistry Aerosol Radiation and Transport (GOCART) model (Ginoux et al., 2001).

In this study, the evaluation is carried out for the forecasts of the innermost domain (domain 4) that has a time-step of 4.4 s. The instantaneous irradiance values are logged every minute while the other WRF outputs are logged every hour. The hourly irradiance, which is used for validation, is obtained by averaging the 60 min-values. As we are interested in the mean hourly irradiance over the whole island, WRF outputs are averaged horizontally. Given the horizontal resolution of the innermost domain (1 km^2) and the surface of Singapore (ca 700 km^2), the island is covered with about 700 cells of domain 4. Using the R package *rworldmap* to determine which cells cover the island, we thus average these 700 cells to get one single hourly value for Singapore for each WRF output variable.

2.3.2. The Global Forecast System (GFS)

The Global Forecast System (GFS) is a global spectral model developed and run by NCEP. Its initial conditions are provided by the Global Data Assimilation System (GDAS). Running at a horizontal spatial resolution of ca. 13 km and with 64 vertical levels, it produces a 2 weeks-ahead forecast every 6 h. Historical forecasts are freely available at a horizontal resolution of 0.5° and, since January 2015, of 0.25°, both with 26 vertical levels. Because part of this work is carried out for year 2014 and for the sake of homogeneity, we only use the coarser resolution of 0.5°. GFS provides initial and boundary conditions for operational implementations of WRF such as the Rapid Refresh (RR or RAP) or the High-Resolution Rapid Refresh (HRRR). Our WRF forecasts are initialized using the 12:00 UTC GFS release (20:00 SGT) and run for 24 h. This allows the model a 12-h spin-up time during the night.

GFS uses a modified version of the Rapid Radiative Transfer Models (Iacono et al., 2008) to predict the global horizontal surface irradiance. It can hence also be used directly to forecast surface irradiance. We use this forecast as a benchmark to demonstrate the efficacy of WRF downscaling. As GFS provides 3-hourly irradiance averages, we need to interpolate the output to hourly values to compare it with WRF. Following Verzijlbergh et al. (2015), we use a clear sky model for this purpose. We first compute the 3-hourly clear sky index as:

$$\langle k_t \rangle_{3h} = \frac{\langle I_{t,GFS} \rangle_{3h}}{\langle I_{t,clear\ sky} \rangle_{3h}} \tag{3}$$

where $\langle I_{t,GFS} \rangle_{3h}$ is the 3 h-average irradiance provided by GFS and $\langle I_{t,clear\ sky} \rangle_{3h}$ the 3 h-average clear sky irradiance computed using Singapore clear sky model of Yang et al. (2014) (see Section 2.2). We then deduce the hourly irradiance:

$$\langle I_{t,GFS} \rangle_{1h} = I_{t,GFS} = \langle k_t \rangle_{3h} \times \langle I_{t,clear\ sky} \rangle_{1h} \tag{4}$$

where $\langle I_{t,clear\ sky} \rangle_{1h}$ is the 1 h-average clear sky irradiance. As we apply multilinear post-processing to GFS, all the other variables (Temperature, Pressure, etc.) also need to be interpolated. We use a simple linear interpolation.

As for WRF, we require a single horizontal value for each GFS output variable. We use a nearest-neighbor approach and average the 4 GFS cells (partially) covering the island.

2.4. Post-processing

We implement a three-steps post-processing system: removal of the yearly and daily cycles, dimensionality reduction, and Model Output Statistic (MOS). In this study, when training is necessary, the results are presented for the year 2016, while the algorithms are trained with the years 2014 and 2015. When no training is necessary (for raw NWP), the results are presented for years 2014, 2015 and 2016.

2.4.1. Clear sky index as the dependent variable

Following the work of Lorenz et al. (2009b) we use the clear sky index as the dependent variable for our MOS. Using k_t as the dependent variable rids the MOS of the burden to resolve the daily and yearly periodic variations of the irradiance due to the position of the Sun.

2.4.2. Model Output Statistic (MOS) and stepwise variable selection

In our case, MOS involves relating the clear sky index $k_{t,MOS}$ to a set of NWP output variables, as per the following relation:

$$\hat{k}_{t,MOS} = \beta_0 + \beta_1 X^t_{NWP,1} + ... + \beta_n X^t_{NWP,n} \tag{5}$$

where $X^t_{NWP,i}$ are outputs of the NWP at time t (or a transformation of these outputs–see Section 2.4.3) and β_i are the corresponding regression coefficients. The regression coefficients can be determined using least square estimation (LSE), which involves minimizing the following cost function:

$$C(\beta_i) = \sum_{t=1}^{T} (k_{t,observed} - \hat{k}_{t,MOS})^2 \tag{6}$$

where $k_{t,observed}$ is the observed clear sky index at time t, and T is the number of time-steps used for training.

There are several ways to choose the explanatory variables $X^t_{WRF,i}$. Univariate regression (UR) is the simplest application of this model as it uses a single explanatory variable, $k_{t,NWP}$. Lorenz et al. (2009b) proposed to fit a 5th order polynomial of the clear sky index and of the cosinus of the zenith angle. Although it gave promising results, this approach is not systematic and information carried by other WRF output variables is lost. We thus choose a different method, introduced for solar irradiance forecasts by Verzijlbergh et al. (2015) and use stepwise variable selection to help select the best possible set of explanatory variables.

Finding the optimum subset of regressors for a given problem (and according to a given criterion) can generally be done only by fitting all possible subsets. However, even nowadays with advances in

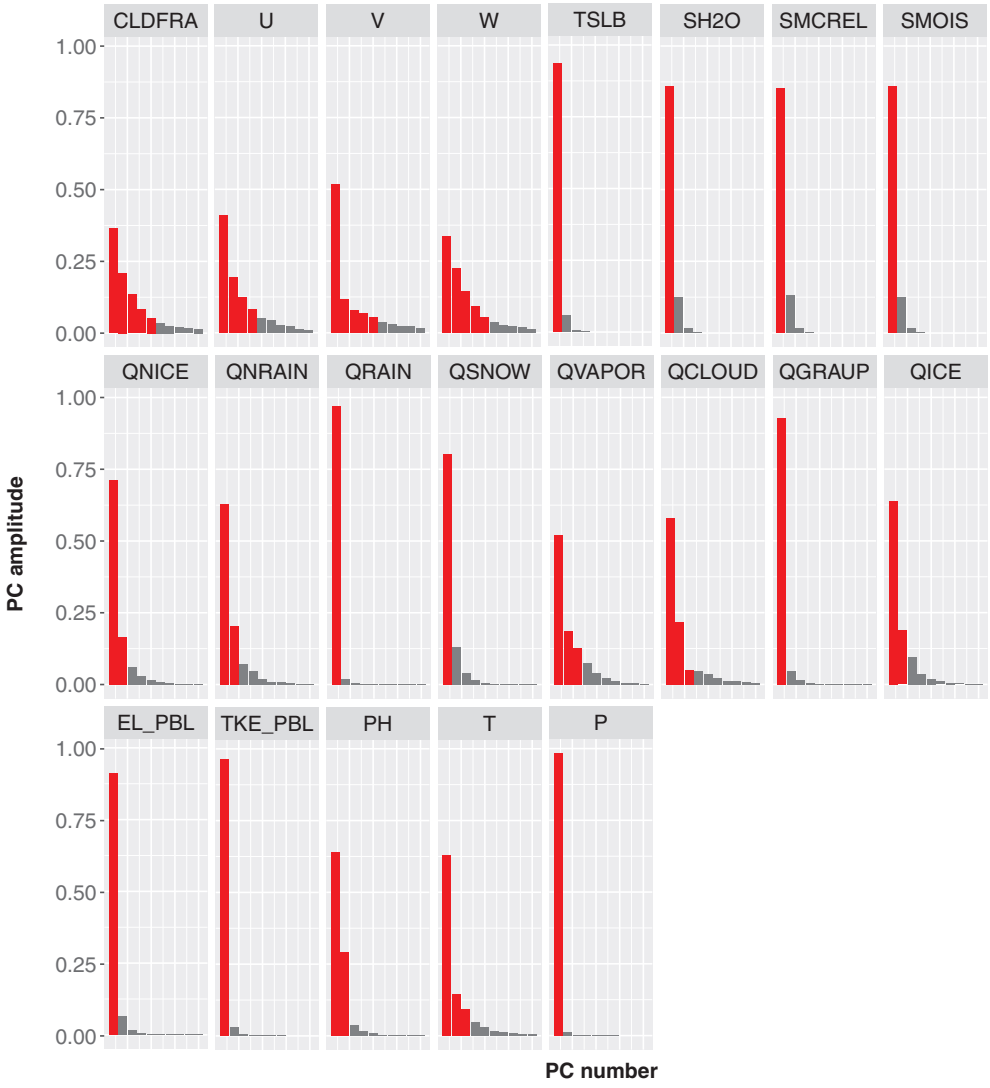

Fig. 3. Result of the Principal Component Analysis (PCA) of WRF-Solar 3D output variables. The 10 largest Principal Components (PCs) are shown for each 3D output variable for WRF-solar. The PCs explaining 80% of the variability of each variable are shown in red. CLDFRA is the cloud fraction; U, V and W are the wind speed components; TSLB, SH2O, SMCREL, and SMOIS are the soil temperature, liquid watter, and relative and absolute moisture; QNICE and QNRAIN are the ice and rain number concentrations; QRAIN, QSNOW, QVAPOR, QCLOUD, QGRAUP and QICE are the rain water, snow, water vapor, cloud water, graupel and ice mixing ratios; EL_PBL and TKE_PBL are the PBL length scale and turbulence kinetic energy; PH is the perturbation geopotential, T the temperature, and P the pressure. (For interpretation of the references to colour in this figure legend, the reader is referred to the web version of this article.)

computational power, it is very impractical to test all possible subsets for sets containing more than 30 variables (that has 2^{30} possible combinations) (Montgomery, 2013). Instead of testing every possible subset, stepwise selection seeks an optimum path through them (Hastie et al., 2009). Starting with only the intercept as regressor, stepwise variable selection iteratively adds and removes regressors based on the resulting multiple regression score. In this work, we use the Bayesian Information Criterion (BIC) (Wilks, 2011). In comparison with other possible model evaluation criteria scores (for example the popular Akaike Information Criterion (AIC) (Montgomery, 2013)), BIC puts a greater penalty on adding new regressors to the model, which we found to give better results. In addition, unlike the F-score used by Verzijlbergh et al. (2015), BIC does not require fine tuning as there is no need for cutoff values. BIC is defined as follow:

$$BIC = n \times ln\left(\frac{SS_{Res}}{n}\right) + p \times ln(n) \tag{7}$$

where n is the number of points, p the number of regressors and SS_{Res} the squared sum of the residuals. At each iteration i of the stepwise selection, let $V^i_{regressors}$ be the subset of variables selected as regressors, $V^i_{candidates}$ the subset of variables not selected as regressors and BIC_i the BIC score of the current subset of regressors. Then:

1. The variable in $V^i_{candidates}$ whose addition to the model would produce the lowest BIC score is removed from $V^{i+1}_{candidates}$ and added to $V^{i+1}_{regressors}$, provided that $BIC_{i+1} < BIC_i$;
2. The variable in $V^i_{regressors}$ whose removal would produce the lowest BIC score is removed from $V^{i+1}_{regressors}$ and added to $V^{i+1}_{candidates}$, provided that $BIC_{i+1} \leqslant BIC_i$.

The algorithm ends when $BIC_{i+1} \geqslant BIC_i$ for any addition of variable and $BIC_{i+1} > BIC_i$ for any removal. In this work, we use the R function *stepAIC* (Venables et al., 2002) that implements a stepwise variable selection with BIC criterion if the degree of freedom is set to $k = log(n)$.

In order to demonstrate the benefit of using multivariate regression, we also apply a simple univariate regression (UR) to each NWP. UR is a special case of MOS where $k_{t,WRF}$ is the only explanatory variable:

$$\hat{k}_{t,MOS} = \beta_0 + \beta_1 k_{t,WRF} \tag{8}$$

where the regression β_0 and β_1 are determined by least square estimation as in Eq. (6).

2.4.3. Dimensionality reduction

WRF and GFS have a large number of output variables: 97, 93 and 77 for WRF-solar, WRF-rrtmg and WRF-dudhia, and 124 for GFS. WRF-solar has more output variables because it computes and logs several aerosol-related variables that are not resolved by WRF-rrtmg nor WRF-dudhia–the 2D aerosol optical depth at 550 nm (TAOD5502D) or the water-friendly aerosol number concentration (QNWFA) for example. Similarly WRF-dudhia outputs less variables than the two other WRF

configurations because the Dudhia scheme is a simplified model that does not resolve certain variables, such as the instantaneous upwelling clear sky shortwave flux (SWUPT), that are logged by RRTMG. The forecast clear sky index, $k_{t,NWP}$–computed as shown in Section 2.2–is also added to the list of potential regressors.

Some of the output variables are in 3 dimensions and are thus defined on several levels–up to 35 for WRF and 26 for GFS. Consequently, the dimension of the output of WRF-solar, WRF-rrtmg, WRF-dudhia and GFS is 754, 665, 649 and 324, respectively. With two years of training only, using this amount of parameters as input of the stepwise variable selection algorithm may lead to some overfitting.

To investigate possible ways to reduce the number of inputs, we conducted a Principal component analysis (PCA) for each 3D output variable of WRF and GFS. PCA transforms the set of vertical levels of each output 3D variable into a set of new levels, called principal components (PCs). The PCs are linear combinations of the original levels and are constructed so that (1) they are *uncorrelated* and (2) the amplitude of each component indicates how much variability of the original set is contained in this component. Fig. 3 shows the 10 largest PCs for each 3D output variable of WRF-solar. We see that more than 80% of every variable vertical levels' variability is contained in at most 5 PCs (highlighted in red). This implies that the vertical levels are highly correlated and suggests that combining the stepwise variable selection algorithm with a previous spatial aggregation procedure could prevent overfitting. In this work, we will consider three alternatives:

1. No dimensionality reduction: all levels of the each 3D variable are used as inputs;
2. 3D variables are averaged vertically: 1 mean value per 3D variable is used as input;
3. For each 3D variable, a PCA is done and only the PC(s) explaining 80% of the variability are taken: 1–5 PC(s) per 3D variable is (are) used as inputs. The selected PC(s) for each 3D output variable of WRF-solar is (are) shown in red in Fig. 3. The variability of most variables can be represented by 1 or 2 PC(s) only, with the exception of wind speed (U,V and W), cloud fraction (CLD), Temperature (T) and water vapor mixing ratio (QVAPOR), that require up to 5 components.

The outputs of this procedure will be used as input for the stepwise variable selection MOS described in the previous section. The naming conventions are summarized in Table 1.

2.5. Forecast evaluation and benchmarks

2.5.1. Metrics of forecast accuracy

The Root Mean Square Error (RMSE) is a widely used metric, defined as follow:

$$\mathrm{RMSE} = \sqrt{\frac{1}{n}\sum_{t=1}^{n}(\hat{I}_{t,forecast} - I_{t,observed})^2} \tag{9}$$

where $I_{t,observed}$ is the observed irradiance at time t, $\hat{I}_{t,forecast}$ the forecasted irradiance and n the number of forecast/observation pairs. As it squares the errors, the RMSE puts a higher penalty on forecasts with high errors; it is appropriate for applications where large errors have a proportionally higher impact than small errors. The Mean Absolute Error (MAE), defined as follow, is more suitable for applications where the cost is proportional to the error (linear cost).

$$\mathrm{MAE} = \frac{1}{n}\sum_{t=1}^{n}|\hat{I}_{t,forecast} - I_{t,observed}| \tag{10}$$

The mean bias error (MBE) and the Pearson correlation coefficient (ρ) are also useful metrics as they can help to achieve a better insight into the forecast behaviour. They are defined by the following equations:

$$\mathrm{MBE} = \frac{1}{n}\sum_{i=t}^{n}(\hat{I}_{t,forecast} - I_{t,observed}) \tag{11}$$

$$\rho = \frac{\mathrm{cov}(I_{observed}, \hat{I}_{forecast})}{\sigma_{I_{observed}}\sigma_{\hat{I}_{forecast}}} \tag{12}$$

where $\mathrm{cov}(I_{observed}, \hat{I}_{forecast})$ is the covariance of $I_{observed}$ and $\hat{I}_{forecast}$, and $\sigma_{I_{observed}}, \sigma_{\hat{I}_{forecast}}$ are the standard deviations of $I_{observed}$ and $\hat{I}_{forecast}$, respectively. The MBE indicates a tendency of the forecast to systematically over-predict or under-predict the irradiance while ρ shows the potential that a univariate linear transformation has to improve a raw forecast. In order to compare a model across regions receiving a different yearly amount of solar energy, the relative counterparts of RMSE, MAE and MBE can be used:

$$\mathrm{rRMSE} = \frac{\mathrm{RMSE}}{\langle I_{observed}\rangle} \tag{13}$$

$$\mathrm{rMAE} = \frac{\mathrm{MAE}}{\langle I_{observed}\rangle} \tag{14}$$

$$\mathrm{rMBE} = \frac{\mathrm{MBE}}{\langle I_{observed}\rangle} \tag{15}$$

Table 1
Naming convention used in this paper.

Name	NWP model	Dimension reduction	Regression procedure
WRF-dudhia-UR	WRF-dudhia	NA	Univariate regression
WRF-dudhia-all	WRF-dudhia	None	Stepwise variable selection
WRF-dudhia-mean	WRF-dudhia	Mean	Stepwise variable selection
WRF-dudhia-PCA	WRF-dudhia	PCA	Stepwise variable selection
WRF-rrtmg-UR	WRF-rrtmg	NA	Univariate regression
WRF-rrtmg-all	WRF-rrtmg	None	Stepwise variable selection
WRF-rrtmg-mean	WRF-rrtmg	Mean	Stepwise variable selection
WRF-rrtmg-PCA	WRF-rrtmg	PCA	Stepwise variable selection
WRF-solar-UR	WRF-solar	NA	Univariate regression
WRF-solar-all	WRF-solar	None	Stepwise variable selection
WRF-solar-mean	WRF-solar	Mean	Stepwise variable selection
WRF-solar-PCA	WRF-solar	PCA	Stepwise variable selection
GFS-UR	GFS	NA	Univariate regression
GFS-all	GFS	None	Stepwise variable selection
GFS-mean	GFS	Mean	Stepwise variable selection
GFS-PCA	GFS	PCA	Stepwise variable selection

where $\langle I_{observed} \rangle = \frac{1}{n} \sum_{i=1}^{n} I_{observed}$ is the average irradiance over the whole dataset. To compare two forecasts, the relative improvement in any of the previous metrics can be useful. The relative improvement in RMSE between $f1$ and $f2$, $R^{f1,f2}$ is given by the following equation:

$$R^{f1,f2} = 100 \times \frac{\mathrm{RMSE}_{f1} - \mathrm{RMSE}_{f2}}{\mathrm{RMSE}_{f2}} \tag{16}$$

A negative $R^{f1,f2}$ indicates that $f1$ has a lower RMSE than $f2$ and is thus more skilled.

According to Lorenz et al. (2016) and Perez et al. (2013), the RMSE should be preferred for power forecasting and grid operation issues. In this work however, we display the overall results in terms of RMSE, MAE, MBE and their relative counterparts. For raw NWP results, we also give the overall correlation. To avoid cluttering, we only use the RMSE or the $R^{f1,f2}$ in figures.

As discussed in Section 2.1, the evaluation is carried out for hourly values of GHI, averaged over Singapore and only zenith angles below 70° are considered.

2.5.2. Significance tests

We use bootstrapping to estimate the statistical significance of a difference between the skill of two forecasts. Bootstrapping estimates the variation of a statistic by resampling with replacement the underlying population. In our case, the statistic is the *difference* in the chosen metric and the population is the forecasting dates and times.

For estimating the statistical significance of e.g. the RMSE difference between any two forecasts $f1$ and $f2$, we proceed as follows. First, 1000 sets of dates are built using resampling with replacement (the resampled sets have the same size as the original set); the difference in RMSE between $f1$ and $f2$ is then computed for each sample; finally, if $\mathrm{RMSE}_{f1} > \mathrm{RMSE}_{f2}$ for N out of 1000 samples, the hypothesis $\mathrm{RMSE}_{f1} > \mathrm{RMSE}_{f2}$ is considered statistically significant with a p value of $N/1000$ (Wilks, 2011). The difference is considered to be statistically significant if $p < 0.05$.

2.5.3. Benchmark models

Smart persistence is one of the most commonly used statistical benchmarks for day-ahead forecasting. It assumes that the sky conditions (represented by the daily average clear sky index $\langle k_t \rangle_{\mathrm{day}}$) do not change from one day to the next, but account for the position of the sun:

$$\hat{I}_{\text{smart pers.}} = \langle k_t \rangle_{\text{previous day}} I_{\text{clear sky}}(t) \tag{17}$$

However, due to the chaotic nature of equatorial weather, it performs poorly in Singapore. We thus also compare our forecasts to a climatological model that assumes an average cloud cover all year long:

$$\hat{I}_{\text{smart climate}} = \langle k_t \rangle_{\text{previous year}} I_{\text{clear sky}}(t) \tag{18}$$

In the case of Singapore, $\langle k_t \rangle_{2015} \approx 0.6$, which corresponds to a partly cloudy sky.

3. Results and discussions

In the results section, we first discuss the performance of WRF irradiance forecasts for different configurations, without post-processing and compare the results with that of raw GFS. We then look at the outcome of the stepwise variable selection for the three alternative dimension reduction techniques and examine how it affects the four NWP forecasts (the three WRF models and GFS). Finally, we compare our best performing model with a smart persistence and a climatological model.

3.1. Raw NWP performance

Fig. 4 shows the time series of the four NWP forecasts–together with the observed and clear sky irradiance–for selected days with different weather types. The RMSE, MAE, MBE and correlation of the four NWP models are shown in Table 2. The four models have a large MBE, which means that they largely overestimate the irradiance, as illustrated in the scatter-plot in Fig. 5. A strong positive bias has already been observed for implementations of WRF with lower resolution (Lara-Fanego et al., 2012b) and for GFS (Perez et al., 2010). In the case of WRF, Ruiz-Arias et al. (2016) hypothesize that it is related to a very low amount of cumulus clouds in the model. Our results show that even with a resolution of 1 km^2, at which we expect the dynamic solver to explicitly resolve cumulus clouds, our WRF models remain biased.

Overall, WRF-dudhia and WRF-solar significantly outperform WRF-rrtmg–in terms of RMSE as well as in terms of MAE. The two former models have statistically indistinguishable RMSE and MAE, which could lead one to conclude that WRF-solar and WRF-dudhia are more similar than WRF-solar and WRF-rrtmg or WRF-rrtmg and WRF-dudhia. However, although their performance is similar, WRF-solar and WRF-dudhia are the most dissimilar forecasts, whereas WRF-rrtmg and WRF-dudhia are the closest. This can be seen in Fig. 5b, c and d that show a scatter plot of WRF-solar versus WRF-rrtmg, WRF-solar versus WRF-dudhia, and WRF-rrtmg versus WRF-dudhia, respectively, as well as the RMSE between each pair of models.

All three configurations of WRF have a lower RMSE, a lower MAE and a higher correlation than GFS overall. Fig. 7 displays the monthly relative RMSE improvement between each WRF configuration and GFS ($R^{WRF,GFS}$). It shows that although GFS performs worst overall, it still has the lowest RMSE for certain months. In general, the performance of WRF is highly correlated with that of GFS (Fig. 6), which is expected as GFS provides the boundary and initial conditions for the WRF models that, as mesoscale models, can only be aware of very large scale phenomena through these conditions.

Fig. 8 decomposes the RMSE of each NWP model for different sky conditions. Every WRF configuration outperforms GFS for every sky condition. The relative difference is biggest for $0.4 < k_t < 0.7$. GFS resolution (ca 13 km) is 13 times coarser than that of our finest WRF domain (1 km). Therefore, considering the importance of convection in Singapore, we should expect WRF to resolve cumulus clouds better than GFS and it is not a surprise that WRF performs much better than GFS for cloudy or partially cloudy conditions.

WRF-rrtmg is outperformed by the two other WRF configurations for every sky conditions. WRF-solar has a small but statistically significant advantage over WRF-dudhia for clear and partly cloudy sky conditions ($k_t > 0.6$) while, on the contrary, WRF-dudhia has a lower RMSE for very cloudy and fully overcast skies ($k_t < 0.4$). This improvement by WRF-solar should not necessarily be a surprise as one big improvement of WRF-solar, the aerosol direct effect on irradiance, is most important for clear skies.

3.2. MOS performance

Tables 3 and 4 show the skill of the post-processed NWP models for univariate and multivariate MOS respectively. Every procedure tested significantly improve the performance of every NWP model. The RMSE is decreased by 24–36%, the MAE by 20–33% and the bias of the post-processed forecast can be as low as −2.9%. While the raw NWP models largely overestimate the irradiance, all the post-processed models but one (WRF-solar-all) slightly underestimate it. As it is the case for univariate as well as for multivariate models, it cannot be as a result of overfitting. We hypothesize that linear regression does not manage to fully capture the dependence of the bias on the NWP outputs variables and slightly overestimates the correction needed for the NWP forecasts.

Our proposed multivariate procedure is statistically significantly better than the univariate reference procedure for GFS, WRF-rrtmg and WRF-solar, but not for WRF-dudhia. The use of a dimensionality reduction technique prior to applying the stepwise variable reduction algorithm has inconsistent results and its relevance depends upon the NWP model and configuration. For GFS, using the vertical mean of 3D

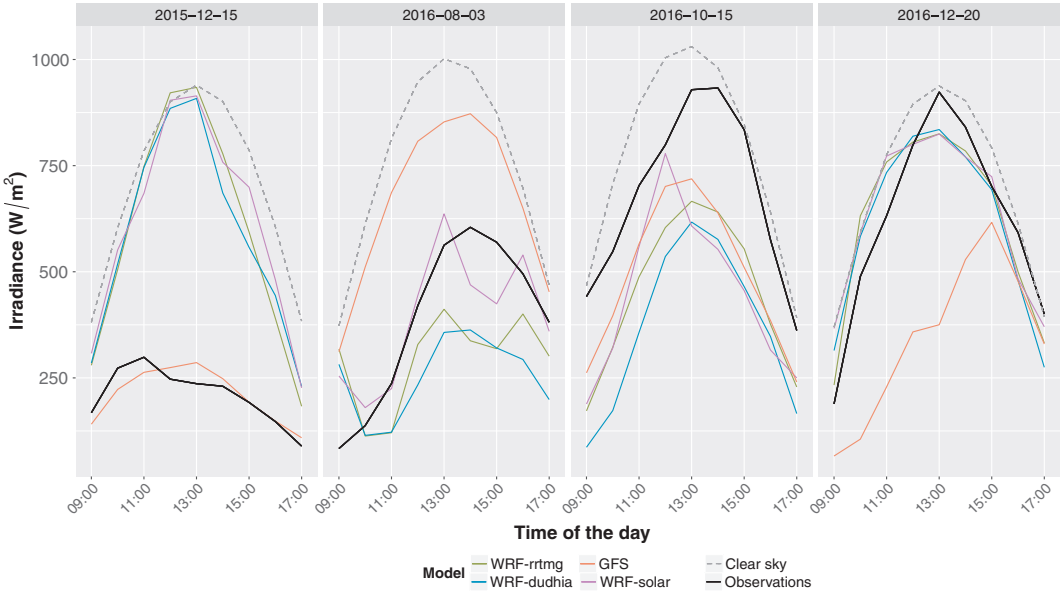

Fig. 4. Time series of the four NWP forecasts for selected days. The observed and clear sky irradiance are displayed in bold and dash lines.

Table 2
Hourly error metrics for GFS, WRF-solar, WRF-dudhia and WRF-rrtmg for years 2014–2016.

	RMSE (W/m^2)	rRMSE (%)	MAE (W/m^2)	rMAE (%)	MBE (W/m^2)	rMBE (%)	ρ
WRF-dudhia	240	50.1	182	37.9	155	32.3	0.68
WRF-rrtmg	258	53.9	203	42.3	185	38.7	0.68
WRF-solar	242	50.4	183	38.2	163	33.9	0.67
GFS	267	55.8	207	43.2	185	38.7	0.64

variables (GFS-mean) is the most successful approach, for WRF-solar the PCA (WRF-solar-PCA) should be preferred, while for WRF-rrtmg, better results are obtained when all the levels are given to the stepwise selection algorithm (WRF-rrtmg-all) (Table 4). Overall, the best performance is achieved by WRF-solar-PCA. Its RMSE is very close to that of GFS-mean and WRF-solar-all, but even though the difference is small, it is statistically significant ($p < 0.02$). Furthermore, the difference in terms of MAE is greater. As RMSE is more sensitive to outliers than MAE, it suggests that WRF-solar is particularly superior to GFS-mean for applications where larger errors do not attract extra penalties.

3.3. Comparison with statistical benchmark models

Table 5 compares the performance of WRF-solar-PCA, our best forecast, with that of a climatological forecast and a smart persistence. WRF-solar-PCA has a lower RMSE, MAE and MBE than the two benchmarks. Fig. 9 shows the monthly RMSE of these three models for 2016; WRF-solar-PCA systematically outperforms smart persistence and it exhibits a lower RMSE than the climatological forecast for 10 months out of 12.

The details of the RMSE for each of the three models and for different sky conditions is given in Fig. 10. WRF-solar-PCA significantly outperforms the smart persistence model for every sky condition. It is also better than the climatological model for fully overcast, partly cloudy and clear sky conditions, and it only has a statistically significantly higher RMSE for kt in [.4,.6]. The RMSE of the two models is statistically indistinguishable for $0.6 < k_t < 0.7$ (overcast and partly cloudy skies). This interval corresponds to average sky conditions in Singapore; as the climatological model assumes average sky condition all the time, it is expected to perform very well under such skies, and is hard to beat in these conditions (similarly, a model assuming constant clear sky would be extremely skilled for $k_t > 0.9$).

4. Conclusion

In this work, an analysis of three different implementations of WRF was conducted. We evaluated the skill of the three models for day-ahead forecasts of Singapore hourly GHI. Two different short wave radiative models were tested with the standard version of WRF and compared with WRF solar; all three models were run at a high resolution of 1 km. In agreement with Zempila et al. (2016), we showed that in terms of RMSE, MAE and MBE, within the suite of options from standard WRF (and with no statistical post-processing) the Dudhia scheme performs better than the RRTMG scheme–although the latter is more sophisticated and computationally expensive. As concluded by Jiménez et al., 2016, we also found that WRF solar is a significant improvement over WRF-standard with RRTMG. Finally, we found that the performance of WRF solar and WRF standard with the Dudhia scheme are statistically indistinguishable, even though the latter performs slightly better for cloudy skies while the former is slightly superior for clear skies.

We also analysed the performance of GFS and showed that without statistical post-processing, WRF is a significant improvement over the global model. It is worth noticing, however, that this is not systematic and that for a few of the tested months, GFS outperforms our three WRF models.

In addition, we developed a new multivariate model output statistics routine that combines stepwise variable selection and dimension reduction techniques. This procedure improves the forecasts for all our models, and the improvement is significantly better than a simple univariate regression for three of our four models. The hierarchy of the models after statistical post-processing is very different from that before post-processing. Before post-processing the models rank as $(\mathrm{RMSE}_{WRF-dudhia}, \mathrm{RMSE}_{WRF-solar}) < \mathrm{RMSE}_{WRF-rrtmg} < \mathrm{RMSE}_{GFS}$, however after post-processing the ranking goes as $\mathrm{RMSE}_{WRF-solar}$

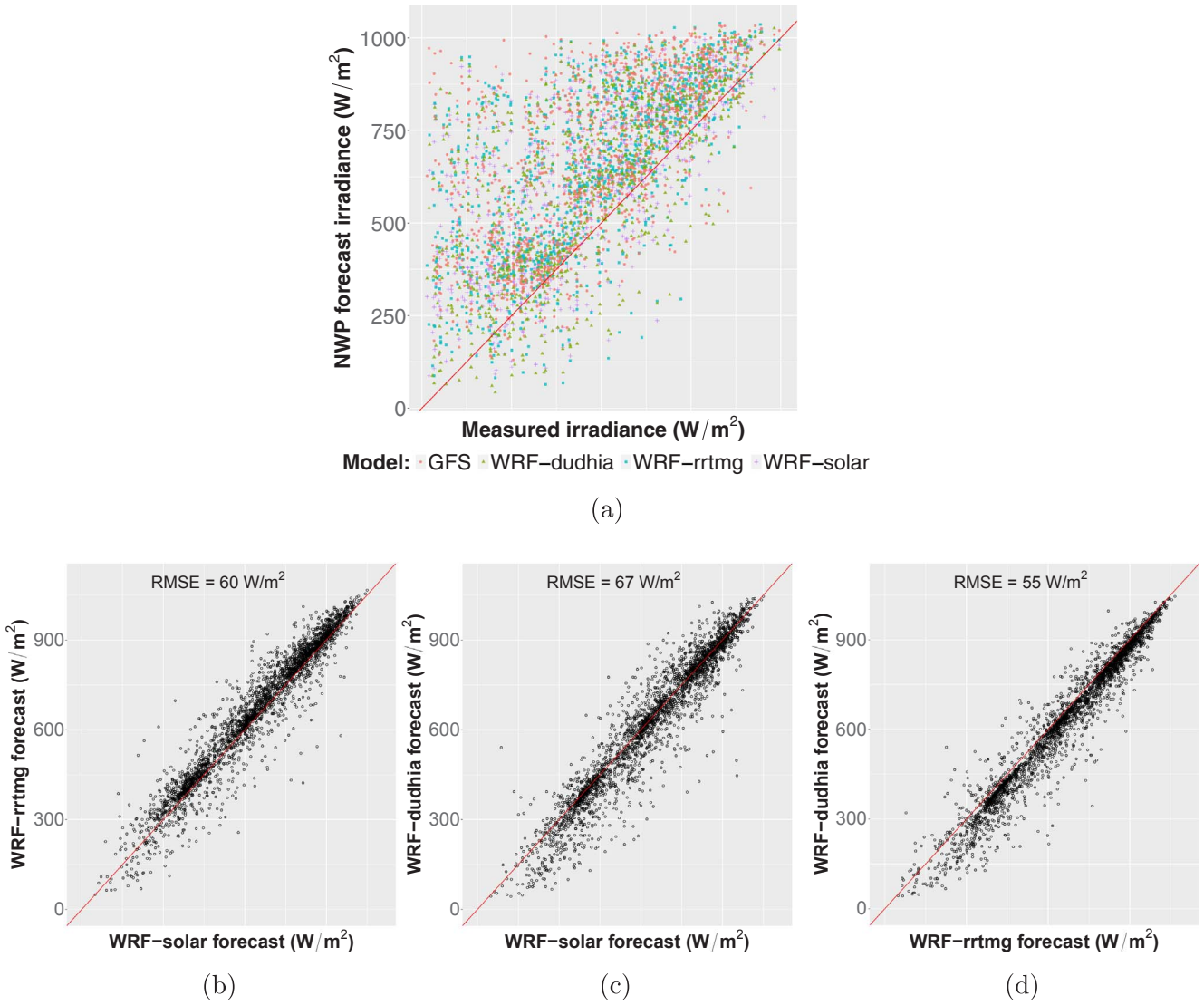

Fig. 5. Scatter plot of forecast irradiance versus observed irradiance for the four NWP models (a) and scatter plots between the three WRF configurations (b, c and d). To reduce clutter, only one day per week is plotted. The identity is plotted in red. (For interpretation of the references to colour in this figure legend, the reader is referred to the web version of this article.)

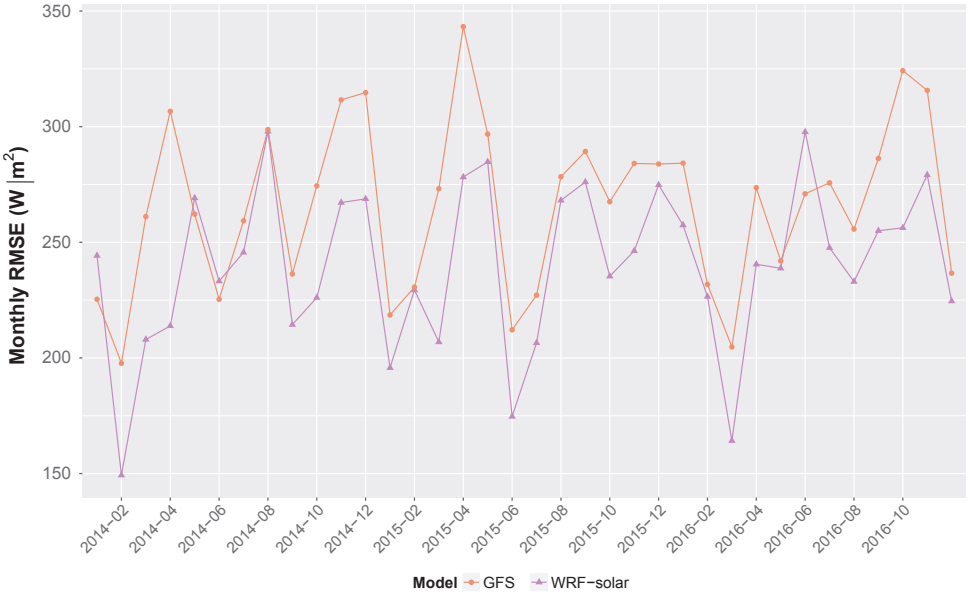

Fig. 6. Monthly RMSE of GFS and WRF-solar from January 2014 to December 2016.

Fig. 7. Monthly RMSE improvement over GFS ($R^{WRF,GFS}$) for WRF-solar, WRF-rrtmg and WRF-dudhia from January 2014 to December 2016.

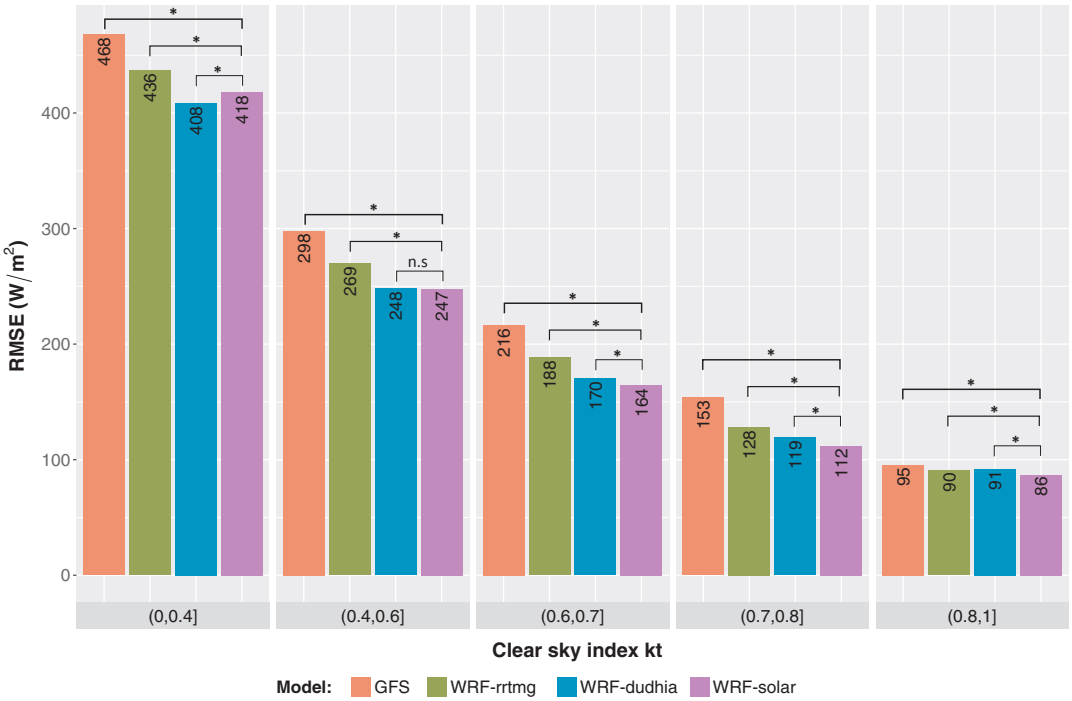

Fig. 8. RMSE of GFS, WRF-solar, WRF-rrtmg and WRF-dudhia as a function of the clear sky index k_t for years 2014, 2015 and 2016. An asterisk indicate a statistically significant difference ($p < 0.05$), while 'n.s.' indicates statistically indistinguishable values. To avoid cluttering, only the difference between WRF-solar and the other models is indicated.

$<\mathrm{RMSE}_{GFS} < (\mathrm{RMSE}_{WRF-rrtmg}, \mathrm{RMSE}_{WRF-dudhia})$. This underlines the need to also compare models after post-processing when conducting a sensitivity study.

Our best model, WRF-solar combined with a PCA and stepwise variable selection, has a relative RMSE of 35.7% and a relative MAE of 28.1%. This is respectively 1 and 5% lower than the best result using GFS (GFS-mean). We demonstrated that the difference, although it is small, is statistically significant. Depending on the application, it may nevertheless not be worth investing in the resources necessary to run WRF at high-resolution and using GFS-mean may be more reasonable. However, it must be highlighted that there are several ways the WRF forecast could be further improved. Firstly, the WRF community is very

Table 3
Hourly error metrics for NWP models combined with UR for year 2016.

	RMSE (W/m^2)	rRMSE (%)	MAE (W/m^2)	rMAE (%)	MBE (W/m^2)	rMBE (%)
WRF-dudhia-UR	179	37.8	147	31.1	−40	−8.5
WRF-rrtmg-UR	181	38.1	149	31.5	−42	−8.8
WRF-solar-UR	179	37.8	147	31.1	−34	−7.2
GFS-UR	183	38.7	152	32.2	−33	−7.0

Table 4
Hourly error metrics for NWP models combined with stepwise variable selection and with the three alternative dimension reduction techniques for year 2016.

	RMSE (W/m^2)	rRMSE (%)	MAE (W/m^2)	rMAE (%)	MBE (W/m^2)	rMBE (%)
WRF-dudhia-all	182	38.3	147	31.0	−57	−12.1
WRF-dudhia-mean	179	37.9	147	31.0	−63	−13.2
WRF-dudhia-PCA	180	38.0	146	30.9	−55	−11.7
WRF-rrtmg-all	173	36.6	141	29.7	−51	−10.9
WRF-rrtmg-mean	178	37.5	145	30.6	−57	−11.9
WRF-rrtmg-PCA	175	36.9	143	30.2	−50	−10.5
WRF-solar-all	178	37.5	137	28.8	19	4.1
WRF-solar-mean	171	36.0	138	29.2	−32	−6.7
WRF-solar-PCA	169	35.7	133	28.1	−14	−2.9
GFS-all	182	38.4	147	31.1	−47	−9.9
GFS-mean	171	36.2	139	29.3	−37	−7.9
GFS-PCA	178	37.7	144	30.4	−45	−9.5

Table 5
Hourly error metrics for WRF-solar-PCA, climatological model and smart persistence for year 2016.

	RMSE (W/m^2)	rRMSE (%)	MAE (W/m^2)	rMAE (%)	MBE (W/m^2)	rMBE (%)
WRF-solar-PCA	169	35.7	133	28.1	−14	−2.9
Smart persistence	220	46.1	170	35.7	−28	−5.9
Climatological model	188	39.4	157	33.0	−26	−5.5

active and new parametrizations are regularly developed, some of which–as WRF-solar–could help improve the forecast. Secondly, and maybe most importantly, WRF can be couped with data assimilation (DA) that takes advantage of local observations that are not and cannot be used by GFS–for example Singapore meteorological stations described in this paper.

Importantly, WRF-solar-PCA is also a significant improvement on the benchmark models. WRF-solar-PCA has RMSE and MAE that are 23% and 22% lower than smart persistence and 10% and 15% lower than the climatological model.

Future work will analyse the sensitivity of irradiance forecast to other physical schemes, such as the cumulus parametrisation schemes or the planetary boundary layer schemes, that also play an important role in predicting irradiance. Furthermore, local and nonlinear regression methods should be investigated.

Acknowledgments

This work has been supported by the Singapore Economic and

Fig. 9. Monthly RMSE for WRF-solar-PCA, climatological model and smart persistence from January to December 2016.

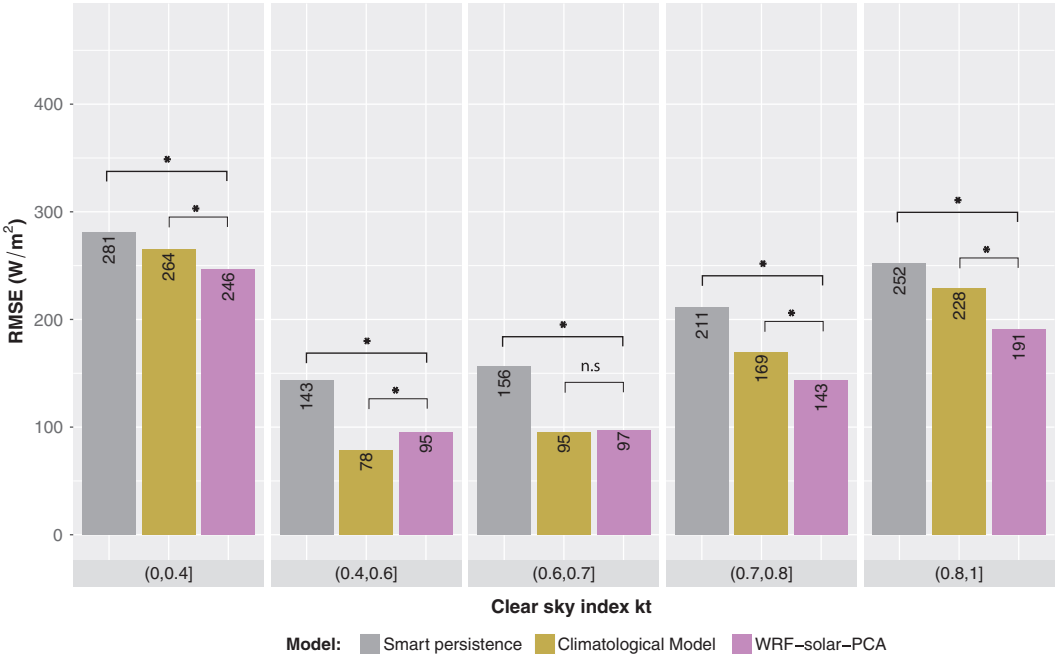

Fig. 10. RMSE of WRF-solar-PCA, climatological model and smart persistence as a function of the clear sky index k_t for year 2016. An asterisk indicate a statistically significant difference ($p < 0.05$), while 'n.s.' indicates statistically indistinguishable values.

Development Board (EDB) under the Weather Intelligence for Renewable Energy EIRP07 grant. The computational work for this article was performed on SERIS High-Performance Computer SGI UV3000 and on resources of the National Supercomputing Centre, Singapore (https://www.nscc.sg). The authors would also like to thank Gerald van der Grijn from MeteoGroup for his remarks and advice, as well as the reviewers for their thorough reviews and constructive comments.

References

Aryaputera, Aloysius W., Verbois, Hadrien, Walsh, Wilfred M., 2016. Probabilistic accumulated irradiance forecast for Singapore using ensemble techniques. In: 2016 IEEE 43rd Photovoltaic Specialists Conference (PVSC). IEEE, pp. 1113–1118 ISBN 978-1-5090-2724-8.

Aryaputera, Aloysius W., Yang, Dazhi, Walsh, Wilfred M., 2015. Day-ahead solar irradiance forecasting in a tropical environment. J. Sol. Energy Eng. 137 (5), 051009 ISSN 0199-6231.

Martinez-Anido, Carlo Brancucci, Botor, Benjamin, Florita, Anthony R., Draxl, Caroline, Lu, Siyuan, Hamann, Hendrik F., Hodge, Bri-Mathias, 2016. The value of day-ahead solar power forecasting improvement. Sol. Energy 129, 192–203 ISSN 0038092X.

Cornaro, C., Pierro, M., Bucci, F., 2015. Master optimization process based on neural networks ensemble for 24-h solar irradiance forecast. Sol. Energy 111, 297–312 ISSN 0038-092X.

Diagne, Maimouna, David, Mathieu, Boland, John, Schmutz, Nicolas, Lauret, Philippe, 2014. Post-processing of solar irradiance forecasts from WRF model at Reunion Island. Sol. Energy 105, 99–108 ISSN 0038092X.

Diagne, Maimouna, David, Mathieu, Lauret, Philippe, Boland, John, Schmutz, Nicolas, 2013. Review of solar irradiance forecasting methods and a proposition for small-scale insular grids. Renew. Sustain. Energy Rev. 27, 65–76 ISSN 13640321.

Dudhia, Jimy, Oct 1989. Numerical study of convection observed during the winter monsoon experiment using a mesoscale two-dimensional model. ISSN 0022-4928. https://doi.org/10.1175/1520-0469(1989)046<3077:NSOCOD>2.0.CO;2.

Ek, M.B., Mitchell, K.E., Lin, Y., Rogers, E., Grunmann, P., Koren, V., Gayno, G., Tarpley, J.D., 2003. Implementation of Noah land surface model advances in the National Centers for Environmental Prediction operational mesoscale Eta model. J. Geophys. Res.: Atmos. 108 (D22). http://dx.doi.org/10.1029/2002JD003296/abstract. n/a–n/a. ISSN 2156-2202.

Ginoux, Paul, Chin, Mian, Tegen, Ina, Prospero, Joseph M., Holben, Brent, Dubovik, Oleg, Lin, Shian-Jiann, 2001. Sources and distributions of dust aerosols simulated with the GOCART model. J. Geophys. Res. 106 (D17), 20255 ISSN 0148-0227.

Glahn, Harry R., Lowry, Dale A., 1972. The use of model output statistics (MOS) in objective weather forecasting. ISSN 0021-8952.

Guarnieri, Ricardo A., Pereira, Enio B., Chou, Sin Chan, 2006. Solar radiation forecast using artificial neural networks in South Brazil. In: Proc. 8 ICSHMO, Apr. 2006, INPE, pp. 1777–1785.

Hastie, Trevor, Tibshirani, Robert, Friedman, Jerome, 2009. The Elements of Statistical Learning Data Mining, Inference, and Prediction, 2nd ed. Springer Series in Statistics Springer, New York, NY ISBN 978-0-387-84858-7.

Iacono, Michael J., Delamere, Jennifer S., Mlawer, Eli J., Shephard, Mark W., Clough, Shepard A., Collins, William D., 2008. Radiative forcing by long-lived greenhouse gases: calculations with the AER radiative transfer models. J. Geophys. Res. Atmos. 113 (13), D13103 ISSN 01480227.

Inman, Rich H., Pedro, Hugo T.C., Coimbra, Carlos F.M., 2013. Solar forecasting methods for renewable energy integration. Prog. Energy Combust. Sci. 39 (6), 535–576 ISSN 03601285.

Jiménez, Pedro A., Alessandrini, Stefano, Haupt, Sue Ellen, Deng, Aijun, Kosovic, Branko, Lee, Jared A., Monache, Luca Delle, Jiménez, Pedro A., Alessandrini, Stefano, Haupt, Sue Ellen, Deng, Aijun, Kosovic, Branko, Lee, Jared A., Monache, Luca Delle, 2016. The role of unresolved clouds on short-range global horizontal irradiance predictability. Mon. Weather Rev. 144 (9), 3099–3107 ISSN 0027-0644.

Jimenez, Pedro A., Hacker, Joshua P., Dudhia, Jimy, Haupt, Sue Ellen, Ruiz-Arias, Jose A., Gueymard, Chris A., Thompson, Gregory, Eidhammer, Trude, Deng, Aijun, 2016. WRF-solar: description and clear-sky assessment of an augmented NWP model for solar power prediction. Bull. Am. Meteorol. Soc. 97 (7), 1249–1264 ISSN 0003-0007.

Kain, John S., Kain, John S., 2004. The Kain–Fritsch convective parameterization: an update. J. Appl. Meteorol. 43 (1), 170–181 ISSN 0894-8763.

Kaur, Amanpreet, Nonnenmacher, Lukas, Pedro, Hugo T.C., Coimbra, Carlos F.M., 2016. Benefits of solar forecasting for energy imbalance markets. Renew. Energy 86, 819–830 ISSN 18790682.

Lara-Fanego, V., Ruiz-Arias, J.A., Pozo-Vázquez, A.D., Gueymard, C.A., Tovar-Pescador, J., 2012a. Evaluation of DNI forecast based on the WRF mesoscale atmospheric model for CPV applications. In: AIP Conference Proceedings, vol. 1477. pp. 317–322 ISBN 9780735410862.

Lara-Fanego, V., Ruiz-Arias, J.A., Pozo-Vázquez, D., Santos-Alamillos, F.J., Tovar-Pescador, J., 2012b. Evaluation of the WRF model solar irradiance forecasts in Andalusia (southern Spain). Sol. Energy 86 (8), 2200–2217 ISSN 0038092X.

Lauret, Philippe, Diagne, Maïmouna, David, Mathieu, 2014. A neural network post-processing approach to improving NWP solar radiation forecasts. Energy Proc. 57, 1044–1052 ISSN 18766102.

Lima, Francisco J.L., Martins, Fernando R., Pereira, Enio B., Lorenz, Elke, Heinemann, Detlev, 2016. Forecast for surface solar irradiance at the Brazilian Northeastern region using NWP model and artificial neural networks. Renew. Energy 87, 807–818 ISSN 09601481.

Lorenz, E., Remund, J., Müller, S.C., Traunmüller, W., Steinmaurer, G., Pozo, D., Ruiz-Arias, J.A., Fanego, V.L., Ramirez, L., Romeo, M.G., Kurz, C., Pomares, L.M., Guerrero, C., 2009a. Benchmarking of different approaches to forecast solar irradiance. In: 24th European Photovoltaic Solar Energy Conference, 21-25 September 2009, Hamburg, Germany, pp. 4199–4208.

Lorenz, Elke, Hurka, Johannes, Heinemann, Detlev, Beyer, Hans Georg, 2009b. Irradiance forecasting for the power prediction of grid-connected photovoltaic systems. IEEE J. Sel. Top. Appl. Earth Obs. Rem. Sens. 2 (1), 2–10 ISSN 1939-1404.

Lorenz, Elke, Kühnert, Jan, Heinemann, Detlev, Nielsen, Kristian Pagh, Remund, Jan, Müller, Stefan C., 2016. Comparison of global horizontal irradiance forecasts based on numerical weather prediction models with different spatio-temporal resolutions. Prog. Photovoltaics: Res. Appl. 24, 1626–1640 ISBN 1099-159X.

Lynch, Peter, 2008. The origins of computer weather prediction and climate modeling. J. Comput. Phys. 227 (7), 3431–3444 ISSN 00219991.

Mathiesen, Patrick, Kleissl, Jan, 2011. Evaluation of numerical weather prediction for intra-day solar forecasting in the continental United States. Sol. Energy 85 (5), 967–977 ISSN 0038092X.
Montgomery, Douglas C., 2013. Introduction to Linear Regression Analysis, 5th ed. set. John Wiley & ons ISBN 9781118780572.
Nakanishi, Mikio, Niino, Hiroshi, 2006. An improved Mellor-Yamada Level-3 model: its numerical stability and application to a regional prediction of advection fog. Bound.-Layer Meteorol. 119 (2), 397–407 ISSN 00068314.
Pelland, Sophie, Galanis, George, Kallos, George, 2013. Solar and photovoltaic forecasting through post-processing of the global environmental multiscale numerical weather prediction model. Prog. Photovoltaics Res. Appl. 21 (3), 284–296 ISSN 10627995.
Perez, Richard, Kivalov, Sergey, Schlemmer, James, Hemker, Karl, Renné, David, Hoff, Thomas E., 2010. Validation of short and medium term operational solar radiation forecasts in the US. Sol. Energy 84 (12), 2161–2172 ISSN 0038092X.
Perez, Richard, Lorenz, Elke, Pelland, Sophie, Beauharnois, Mark, Van Knowe, Glenn, Hemker, Karl, Heinemann, Detlev, Remund, Jan, Müller, Stefan C., Traunmüller, Wolfgang, Steinmauer, Gerald, Pozo, David, Ruiz-Arias, Jose a., Lara-Fanego, Vicente, Ramirez-Santigosa, Lourdes, Gaston-Romero, Martin, Pomares, Luis M., 2013. Comparison of numerical weather prediction solar irradiance forecasts in the US, Canada and Europe. Sol. Energy 94, 305–326 ISSN 0038092X.
Pierro, M., Bucci, F., Cornaro, C., Maggioni, E., Perotto, A., Pravettoni, M., Spada, F., 2015. Model output statistics cascade to improve day ahead solar irradiance forecast. Sol. Energy 117, 99–113.
Ruiz-Arias, José A., Arbizu-Barrena, Clara, Santos-Alamillos, Francisco J., Tovar-Pescador, Joaquín, Pozo-Vázquez, David, 2016. Assessing the surface solar radiation budget in the WRF model: a spatiotemporal analysis of the bias and its causes. Mon. Weather Rev. 144 (2), 703–711 ISSN 0027-0644.
Skamarock, W.C., Klemp, J.B., Dudhi, J., Gill, D.O., Barker, D.M., Duda, M.G., Huang, X.-Y., Wang, W., Powers, J.G., 2008. MOS, Technical Report (June): 113. ISSN 1477870X.
Thompson, Gregory, Eidhammer, Trude, 2014. A study of aerosol impacts on clouds and precipitation development in a large winter cyclone. J. Atmos. Sci. 71 (10), 3636–3658 ISSN 0022-4928.
Venables, W.N., Ripley, B.D., 2002. Modern applied statistics with S. Technometrics 45 (1), 111 ISSN 0040-1706.
Verzijlbergh, Remco A., Heijnen, Petra W., de Roode, Stephan R., Los, Alexander, Jonker, Harm J.J., 2015. Improved model output statistics of numerical weather prediction based irradiance forecasts for solar power applications. Sol. Energy 118, 634–645 ISSN 0038092X.
Wilks, Daniel S., 2011. Statistical Methods in the Atmospheric Sciences. Academic Press ISBN 9780123850232.
Yang, Dazhi, Walsh, Wilfred M., Jirutitijaroen, Panida, 2014. Estimation and applications of clear sky global horizontal irradiance at the equator. J. Sol. Energy Eng. 136 (3), 034505 ISSN 0199-6231.
Zamora, Robert J., Dutton, Ellsworth G., Trainer, Michael, McKeen, Stuart A., Wilczak, James M., Hou, Yu-Tai, 2005. The accuracy of solar irradiance calculations used in mesoscale numerical weather prediction. Mon. Weather Rev. 133 (4), 783–792 ISSN 0027-0644.
Zempila, Melina-Maria, Giannaros, Theodore M., Bais, Alkiviadis, Melas, Dimitris, Kazantzidis, Andreas, 2016. Evaluation of WRF shortwave radiation parameterizations in predicting global horizontal irradiance in Greece. Renew. Energy 86, 831–840 ISSN 0960148.